Random band-edge model description of thermoelectricity in high-mobility disordered semiconductors: application to amorphous oxide In-Ga-Zn-O

Ivan I. Fishchuk,[1] Andrey Kadashchuk,[2,3,†] Cedric Rolin,[3] Heinz Bässler,[4] Anna Köhler,[4,5] Paul Heremans,[3] and Jan Genoe[3]

[1] *Institute for Nuclear Research, National Academy of Sciences of Ukraine, Prospect Nauky 47, 03680 Kyiv, Ukraine*

[2]*Institute of Physics, National Academy of Sciences of Ukraine, Prospect Nauky 46, 03028 Kyiv, Ukraine*

[3]*IMEC, Kapeldreef 75, B-3001 Leuven, Belgium*

[4]*Bayreuth Institute of Macromolecular Research (BIMF), University of Bayreuth, Universitätsstr. 30, 95448 Bayreuth, Germany*

[5]*Soft Matter Optoelectronics and Bavarian Polymer Institute (BPS), University of Bayreuth, Universitätsstr. 30, 95448 Bayreuth, Germany*

[†] *corresponding author:* Andriy.Kadashchuk@imec.be

Abstract

Unraveling the dominant charge transport mechanism in high-mobility amorphous oxide semiconductors is still a matter of controversy. In the present study we extended the random band-edge model suggested before for the charge transport and Hall-effect mobility in such disordered materials [Fishchuk *et al*., Phys. Rev. B **93**, 195204 (2016)], and also describe the field-effect-modulated thermoelectricity in amorphous In-Ga-Zn-O (a-IGZO) films under the same premises. The model is based on the concept of charge transport through the extended states and assumes that the transport is limited by the spatial variation of the position of the band edge due to the disorder potential, rather than by localized states. The theoretical model is formulated using the Effective Medium approximation framework and describes well basic features of the Seebeck coefficient in disordered materials as a function of energy disorder, carrier concentration and temperature. Carrier concentration dependences of power factor and thermoelectric figure of merit have been also considered for such systems. Besides, our calculations reveal a remarkable turnover effect from a negative to a positive temperature dependence of Seebeck coefficient upon increasing carrier concentration. The suggested unified model provides a good quantitative description of available experimental data on the Seebeck coefficient and the charge mobilities measured in the same a-IGZO transistor as a function of the gate voltage and temperature by considering the same charge transport mechanisms. This promotes a deeper understanding and a more credible and accurate description of the transport process in a-IGZO films.

I. INTRODUCTION

Understanding the thermoelectric properties of amorphous semiconducting materials is important not only for technological development of thermoelectric devices, but also from a fundamental standpoint as it can provide unique and complementary insight into the underlying mechanism of the electronic transport in these materials. Thermoelectric properties are conventionally probed via measuring the Seebeck coefficient, α, (also referred to as thermopower) that is defined as $\alpha = \Delta V/\Delta T$, where ΔV is the thermoelectric voltage (or electromotive force) generated in a material in response to an applied temperature differential ΔT. The Seebeck coefficient not only governs the efficiency of thermoelectric converters – the study of field-effect-modulated Seebeck coefficients has been also suggested as a new characterization method to investigate the charge carrier transport in disordered semiconductors [1]. An important advantage is that the Seebeck voltage is independent of the interfacial contact [2], therefore the Seebeck effect is considered as a novel way to uncover the intrinsic characteristics of the charge-carrier transport [3]. Thus, thermoelectricity in conjunction with the charge mobility measurements complements the conventional field-effect transistor (FET) characterization approach and can therefore promote a more accurate theoretical description of transport process as both phenomena are to be premised on the same physical mechanism.

Amorphous metal oxide InGaZnO (a-IGZO) introduced by Nomura *et al.* [4] in the early 2000s has enormous potential as n-type semiconductor material for the realization of the next generation of thin-film transistor (TFT) technology [5] due to its greatly improved charge transport properties, superior spatial uniformity, high transparency in the whole visible range, and relatively low temperature deposition compatible with plastic substrates for flexible electronics and flat-panel displays. Another emerging application of a-IGZO relates to realization of transparent and flexible thermoelectric modules [6-9], as e.g., future power supply for the internet of things [6], for wearable heating and for cooling devices. Several amorphous metal oxides, including a-IGZO, have recently been proposed as promising thermoelectric materials due to their mechanical properties, low lattice thermal conductivity (inherent to amorphous materials) [10], and relatively large thermopower and electron mobility. A low processing temperature and possibility of thin-film device fabrication on large areas with low cost is another merit for thermoelectric application. a-IGZO is an intrinsically energetically disordered solid due to the constituting ions are statistically distributed at the lattice sites. Yet, it features a remarkably high charge-carrier mobility (μ~10-50 cm^2/Vs) for a disordered material [4,11] being at least an order of magnitude greater than in amorphous silicon (<1 cm^2/Vs). This is due to the fact that the bottom of the conduction band of

a-IGZO is composed of spatially spread metal *s*-orbitals with spherically symmetric shape, which are weakly influenced by the amorphization and consequently result in a much lower density of localized states in this material.

In spite of a large amount of work having been done on the charge transport studies in this material for the last decade, its theoretical description is still far from complete. Although a-IGZO films show a well-developed free-electron-like Hall effect [4,12,13], suggesting thereby that the mobile charge carriers are actually delocalized, both Hall and drift FET mobilities typically exhibit a thermally activated behavior ($d\mu/dT > 0$) and increase with increasing carrier concentration, which cannot be rationalized by classical band transport motion. Furthermore, measurements of the field-effect-modulated thermopower in a-IGZO have revealed that the Seebeck coefficient features a remarkably weak temperature dependence, while it decreases significantly with increasing the carrier concentration in FET devices. [14]. The basic charge transport mechanism in a-IGZO is still a matter of controversy - several alternative theoretical concepts were suggested to date, including band-like transport with random barriers [4,12-17], trap-limited transport within the multiple trapping and release (MTR) model [18,19], hopping transport [14], and the random band-edge model based on either the effective medium approximation (EMA) [20] or percolation concepts [21]. These mechanisms and their combinations were typically used to describe a limited set of experimental measurements, while a unified theoretical framework capable of describing the *full properties of charge transport* in a-IGZO (such as drift charge-carrier mobility, Hall mobility, electrical conductivity, and Seebeck coefficient as a function of disorder, carrier concentration and temperature) is still missing.

Recently, Nenashev *et al.* [21] and Baranovskii *et al.* [22] presented a critical analysis of different mechanisms and theoretical frameworks that were suggested in literature for the description of the charge transport in a-IGZO semiconductor. They can be categorized as follows. Band transport affected by random potential barriers (RB concept) was first suggested as dominant mechanism by Kamiya and Nomura [12-15] using percolation arguments proposed by Adler [23] to describe the temperature- and carrier-concentration dependences of charge transport, including also thermoelectric characteristics in a-IGZO [14]. The concept of the band transport via delocalized states is supported by the observations of a well-developed Hall effect, which points at the essential occupation of bandlike states [12,13,21]. The RB model assumes that the charge-carriers move above the band edge ε_m and their transport is hindered by the presence of random potential barriers created by the disorder potential above the ε_m. However, as pointed out in Ref. [21], if disorder

creates potential *barriers above the band edge*, it will inevitably create potential *wells below the band edge*, which was ignored in the RB-based Kamia-Nomura model. The statistical distribution of these wells must be taken into account [21], which makes ε_m a random quantity, which is in variance to the RB model where it has been treated as a constant. Another serious shortcoming of the Kamia-Nomura approach [12-15] is that, despite their claim, the percolation nature of the conduction process has not been properly taken into account in their formalism, as pointed out in Ref. [21, 22]. The percolation transport problem has been recently thoroughly reinvestigated withing the RB concept [22], and the results of Kamia-Nomura approach were found to be in sharp contrast to that obtained within an established percolation theory. Besides, the Kamia-Nomura model overestimates the Seebeck coefficient in a-IGZO and predicts a much stronger temperature dependence $\alpha(T)$ as compared to experimental observations [14].

A trap-limited band transport in terms of the multiple trapping and release (MTR) model has also been considered as a possible transport mechanism in a-IGZO [18, 19, 24]. It assumes that most of the carriers are trapped in the defect-induced localized states below the ε_m and that the transport is controlled by thermal release of carrier to the band states. However, Germs *et al.* argued [14] that not the MTR transport, but rather the interplay between the hopping and the band transport should be considered as the appropriate transport mechanism in a-IGZO materials. They claimed that the charge transport is dominated by variable range hopping below, rather than by bandlike transport above the mobility edge [14]. An important drawback of the hopping model description of the charge mobility measured in a-IGZO is that it requires an unusually large value of the charge localization length in the tail states, about 4.8 nm [14], that exceeds by far the estimates for the localization length of carriers in the band tails of inorganic semiconductors [21]. Besides, the FET mobility in a-IGZO virtually coincides with the mobility obtained from the Hall measurements, which is incompatible with the notion of dominant hopping transport regime. On the other hand, the experimentally evaluated activation energies of FET mobility, which is associated with the energy difference between the Fermi level and the ε_m, turned out to be as low as ∼10–40 meV, i.e., $\leq 3k_BT$, in optimized a-IGZO devices at sufficiently large gate voltages [13,20,25]. According to the Fermi-Dirac statistics this implies a significant degeneration in such semiconductor at room temperature as a large fraction of charge carriers would populate the delocalized states above ε_m. Thus, it is obvious that the MTR formalism can hardly be applicable in the case when the Fermi level is very close to the conduction band edge. Besides, the MTR model predicts [26] a markedly stronger increase of Seebeck coefficient in a-IGZO with

temperature, as compared with experiment [14] which shows a very weak temperature dependence.

Shortcomings of the band-transport Kamia-Nomura model might be eliminated in the "random band-edge" model recently suggested by Fishchuk *et al.* [20], which combines band transport and localized band-tail states. Significant modification made in this model is that, instead of the distribution of potential barriers above a *constant* global band edge ε_m postulated in Kamia-Nomura model [12-15], the random band-edge model assumes that the disorder potential causes random long-range variations of the band edge, i.e., the ε_m is a variable. The latter has been also verified by the first-principles calculations in a-IGZO [20]. It was further assumed that spatial fluctuations of ε_m are described by a Gaussian distribution with standard deviation δ in terms of the Thomas-Fermi approximation [27]

$$g\left(\varepsilon_m\right)=\frac{1}{\delta\sqrt{2\pi}}\exp\left[-\frac{1}{2}\left(\frac{\varepsilon_m}{\delta}\right)^2\right], \tag{1}$$

where the position of the ε_m is counted from the position of the band edge without disorder potential. Thus δ can be considered as a measure of the band-edge disorder. Nenashev *et al.* [21] pointed to this concept as the most appropriate for amorphous oxide semiconductors and used it to formulate their percolation theory for description of the drift charge mobility and conductivity in a-IGZO.

It is worth noting that a similar concept has been widely applied to heavily doped and highly compensated semiconductors [27,28], and represents an alternative to more common band-tail state descriptions of the charge transport in chalcogenide glasses [29] and amorphous silicon α-Si:H [30,31]. Notably, a random band-edge model has been also formulated to describe the influence of lateral variations of band-gap energies Eg in semiconductor alloys on radiative efficiency limits of solar cells [52]. The authors argue that band-gap nonuniformities can arise, e.g., in compound semiconductors, because of changes of the material stoichiometry across the cell or module area, likewise in semiconductors alloys because of composition variations. A Gaussian distribution, similar to Eq. (1), was assumed and its standard deviation δ_{Eg} was taken as a measure for the fluctuations [52]. It was demonstrated that fluctuations degrade the achievable efficiency of solar cells – the calculated maximum efficiency was found to decrease by about 1.7% and 6.1% with respect to a uniform band gap when δ_{Eg} increases from 50 to 100 meV, respectively [52]. Currently, this approach is widely used to describe the operation of solar cells made from

organic materials, hybrid organic-inorganic perovskites, etc. [53, 54]. Interestingly, for the lead-halide perovskite cells, δ_{Eg} varies from 17 to 35 meV, resulting in smaller corresponding voltage losses [54]. We recently applied the random band-edge model also to weakly disordered high-mobility organic semiconductors with delocalized nature of charge transporting states [35].

The possible reason for band-edge disorder in a-IGZO might be envisioned as follows. The spatial spread of the s-orbitals is sufficiently large in a-IGZO exceeding the inter-cation distance, which gives rise to direct overlap among s-orbitals of neighboring metals [4]. Due to the spherical shape of these orbitals, the overlap is basically insensitive to structural-randomness-induced distribution of bond angles and is maintained in the disordered amorphous structure. This leads to charge delocalization within electron pathways dominantly constituted by the metal orbitals in a-IGZO. One might imagine that a variation in delocalized electron pathway size results in a corresponding variation in their conduction band-edge energies. This is reminiscent of organic semiconducting conjugated polymers where the variation in the effective conjugation lengths of segments, over which the excitation can delocalize in a coherent manner, gives rise to variation in their electronic state energies [36].

Fishchuk *et al.* [20] have applied the random band-edge concept to formulate a theoretical framework based on the Effective Medium Approximation (EMA) method to describe universally effective drift and Hall mobility in heterogeneous materials as a function of disorder, temperature, and carrier concentration within the same theoretical formalism. The EMA description has been successfully applied to describe experimental results on the charge transport measured in a-IGZO. In particular, the model reproduces well both the conventional Meyer-Neldel compensation behavior for the charge-carrier mobility and an inverse-MN effect for the conductivity observed experimentally in a-IGZO TFTs. The band-edge disorder parameter δ=40 meV and the conduction-band mobility μ_0=22 cm^2/Vs has been inferred by fitting experimental results using the EMA approach [20], which turned out to be quite close to the values δ=50 meV and μ_0=36 cm^2/Vs obtained by Nenashev *et al.* [21] using their percolation theory. This shows that there is not much difference between the results of the percolation theory and those of the EMA for the range of parameters relevant to the experimental situation studied in Ref. [20]. Therefore, we consider these approaches as complementary.

In this paper, the random band edge concept is applied for the first time to develop a theoretical description of the thermoelectric properties of amorphous oxide semiconductors using the EMA approach. We find that our model can describe well the available experimental data on both

Seebeck coefficients and the drift charge-carrier mobilities measured as a function of charge-carrier density and temperature in the same a-IGZO transistor. Previously this concept was used to also describe the Hall mobility in this material [20]. This implies that the suggested EMA framework can describe the full properties of the charge transport in the a-IGZO semiconductor, premised on the same concept of the random band edge variation and same material parameters.

II. THEORETICAL FORMULATIONS

To consider field-effect-modulated thermoelectric properties of a-IGZO films, we adopt the random band-edge model suggested before in Ref. [20]. The model assumes that the position of the band edge ε_m varies in space due to disorder potential according to a Gaussian distribution given by Eq.(1). The density of extended (band) states at $\varepsilon > \varepsilon_m$ is usually approximated as

$$D(\varepsilon) = D_0\sqrt{\varepsilon - \varepsilon_m}\ , \quad (2)$$

where coefficient $D_0 = \left(2m^*\right)^{3/2} / 2\pi^2\hbar^3$ is defined by the effective mass $m*$. For a-IGZO thin films, $D_0 = 10^{21} cm^{-3} eV^{-3/2}$ has been reported before [37]. Following Ref. [20], in our treatment we only take into account delocalized states and energy distribution of ε_m in the form of Eq. (1), while the presence of localized states below $\varepsilon < \varepsilon_m$ is neglected for simplicity.

For a given value ε_m, in the general case of applied electric field and a sufficiently small temperature gradient, a corresponding local electric current density $\mathbf{J}(\varepsilon_m)$ can be presented as a linear function of both local electric field $\mathbf{E}(\varepsilon_m)$ and temperature field (gradient) $\mathbf{G}(\varepsilon_m)$ [38,39]

$$\mathbf{J}(\varepsilon_m) = \sigma(\varepsilon_m)\mathbf{E}(\varepsilon_m) + \beta(\varepsilon_m)\mathbf{G}(\varepsilon_m). \quad (3)$$

where $\sigma(\varepsilon_m)$ is the local electrical conductivity and $\beta(\varepsilon_m)$ is a scalar coefficient independent of either $\mathbf{E}(\varepsilon_m)$ or $\mathbf{G}(\varepsilon_m)$. Configurational averaging in the left and right parts of Eq.(3) over the energy distribution of ε_m (Eq. (1)) yields

$$\langle \mathbf{J}(\varepsilon_m) \rangle = \sigma_e \langle \mathbf{E}(\varepsilon_m) \rangle + \beta_e \langle \mathbf{G}(\varepsilon_m) \rangle\ . \quad (4)$$

Here σ_e is the effective electrical conductivity and β_e is an effective coefficient introduced above phenomenologically. Under an open circuit condition $\langle \mathbf{J}(\varepsilon_m) \rangle = 0$, Eq. (4) leads to

$\langle \mathbf{E}(\varepsilon_m) \rangle = \alpha_e \langle \mathbf{G}(\varepsilon_m) \rangle$, where α_e is the effective Seebeck coefficient defined as $\alpha_e = -\beta_e / \sigma_e$. Thus, to obtain the effective Seebeck coefficient, we need to calculate the effective values of σ_e and β_e, and for that we employ the Effective Medium approximation (EMA) formalism.

EMA approach suggested earlier by Kirkpatrick [40] and also verified by our group [41] is a particularly useful method for calculating the effective conductivity in weakly and moderately disordered systems. It is based on the following self-consistency equation allowing determining the effective conductivity σ_e from its local values $\sigma(\varepsilon_m)$

$$\left\langle \frac{\sigma(\varepsilon_m) - \sigma_e}{\sigma(\varepsilon_m) + (d-1)\sigma_e} \right\rangle = 0, \tag{5}$$

where d is the spatial dimension. Hereafter we consider a three-dimensional (3D) system. Here the angular brackets mean the averaging over the density distribution function $g(\varepsilon_m)$:

$$\langle A_m \rangle \equiv \int_{-\infty}^{\infty} d\varepsilon_m g(\varepsilon_m)\, A_m. \tag{6}$$

The local electrical conductivity $\sigma(\varepsilon_m)$ can be calculated from the energy integral as [38,39]

$$\sigma(\varepsilon_m) = -\frac{e^2}{3} \int_{\varepsilon_m}^{\infty} D(\varepsilon)\tau(\varepsilon)v^2(\varepsilon) \frac{\partial f(\varepsilon)}{\partial \varepsilon} d\varepsilon, \tag{7}$$

where e is the charge of the electron, $\tau(\varepsilon)$ is the energy-dependent scattering relaxation time, and $v(\varepsilon)$ is Fermi velocity. Here $f(\varepsilon)$ is the Fermi-Dirac distribution:

$$f(\varepsilon) = \frac{1}{1 + \exp\left(\frac{\varepsilon - \varepsilon_F}{k_B T} \right)}, \tag{8}$$

where ε_F is the Fermi level, which is determined by solving the following equation for the total charge-carrier concentration n:

$$n = \int_{-\infty}^{\infty} d\varepsilon_m g(\varepsilon_m) \int_{\varepsilon_m}^{\infty} d\varepsilon D(\varepsilon) f(\varepsilon). \tag{9}$$

Eq. (7) can be rewritten as follows:

$$\sigma(\varepsilon_m) = \frac{2e^2}{3m^*} \frac{D_0}{k_B T} \int_{\varepsilon_m}^{\infty} (\varepsilon - \varepsilon_m)^{3/2} \tau(\varepsilon) f(\varepsilon) [1 - f(\varepsilon)] d\varepsilon \tag{10}$$

Then we represent Eq. (10) in the form

$$\sigma\left(\varepsilon_m\right)=\frac{2e^2}{3m^*}\frac{D_0}{k_BT}\left\langle\tau\left(\varepsilon_m\right)\right\rangle_1\int_{\varepsilon_m}^{\infty}\left(\varepsilon-\varepsilon_m\right)^{3/2}f\left(\varepsilon\right)\left[1-f\left(\varepsilon\right)\right]d\varepsilon, \tag{11}$$

where

$$\left\langle\tau\left(\varepsilon_m\right)\right\rangle_1=\frac{\int_{\varepsilon_m}^{\infty}\left(\varepsilon-\varepsilon_m\right)^{3/2}\tau\left(\varepsilon\right)f\left(\varepsilon\right)\left[1-f\left(\varepsilon\right)\right]d\varepsilon}{\int_{\varepsilon_m}^{\infty}\left(\varepsilon-\varepsilon_m\right)^{3/2}f\left(\varepsilon\right)\left[1-f\left(\varepsilon\right)\right]d\varepsilon}\ . \tag{12}$$

Generally, if the functional dependence for the energy-dependent scattering time $\tau\left(\varepsilon\right)$ is known, one can calculate the effective conductivity by substituting Eq. (11) in (5). However, the $\tau\left(\varepsilon\right)$ may also depend on temperature and carrier concentration in the case of degeneracy, therefore its determination is not a trivial task and requires a separate thorough study of the mechanism of the electron scattering in the material of interest. Therefore, following Refs.[20,21] we assume for simplicity a constant $\left\langle\tau\left(\varepsilon_m\right)\right\rangle_1=\tau_1$ under the applied electric field. This can be done by setting $\varepsilon_m=0$ in Eq.(12), analogously to an ordered system. We further consider τ_1 as a fitting parameter.

Further, the effective coefficient β_e can be calculated using an alike EMA self-consistency equation:

$$\left\langle\frac{\beta\left(\varepsilon_m\right)-\beta_e}{\beta\left(\varepsilon_m\right)+\left(d-1\right)\beta_e}\right\rangle=0\,. \tag{13}$$

In this case coefficient $\beta\left(\varepsilon_m\right)$ can be expressed as [38,39]

$$\beta\left(\varepsilon_m\right)=-\frac{e}{3}\int_{\varepsilon_m}^{\infty}D\left(\varepsilon\right)\tau\left(\varepsilon\right)v^2\left(\varepsilon\right)\frac{\partial f\left(\varepsilon\right)}{\partial\varepsilon}\frac{\varepsilon-\varepsilon_F}{T}d\varepsilon\,. \tag{14}$$

It can be then rewritten in the form

$$\beta\left(\varepsilon_m\right)=\frac{2ek_B}{3m^*}\frac{D_0}{\left(k_BT\right)^2}\left\langle\tau\left(\varepsilon_m\right)\right\rangle_2\int_{\varepsilon_m}^{\infty}\left(\varepsilon-\varepsilon_m\right)^{3/2}\left(\varepsilon-\varepsilon_F\right)f\left(\varepsilon\right)\left[1-f\left(\varepsilon\right)\right]d\varepsilon\,, \tag{15}$$

where

$$\left\langle \tau\left(\varepsilon_m\right)\right\rangle_2 = \frac{\int\limits_{\varepsilon_m}^{\infty} \left(\varepsilon-\varepsilon_m\right)^{3/2} \tau\left(\varepsilon\right)\left(\varepsilon-\varepsilon_F\right) f\left(\varepsilon\right)\left[1-f\left(\varepsilon\right)\right] d\varepsilon}{\int\limits_{\varepsilon_m}^{\infty} \left(\varepsilon-\varepsilon_m\right)^{3/2} \left(\varepsilon-\varepsilon_F\right) f\left(\varepsilon\right)\left[1-f\left(\varepsilon\right)\right] d\varepsilon} . \quad (16)$$

Similarly to electrical conductivity, the effective temperature-induced conductivity β_e can be calculated by substituting Eq. (15) in (13). However, due to the lack of information about material-specific electron scattering mechanism, we assume a constant electron scattering time $\left\langle \tau\left(\varepsilon_m\right)\right\rangle_2 = \tau_2$ by setting $\varepsilon_m = 0$ in Eq. (16), and consider τ_2 also as a fitting parameter. It worth noting that energy-independent τ was also assumed in Ref. [14, 42] where the authors use $\tau\left(\varepsilon\right) = \tau_0$ and thereby $\tau_1 = \tau_2 = \tau_0$. Note, that since Eq.(12) and (16) are not equivalent, it is obvious that in general case $\tau_1 \neq \tau_2$ provided that the dependence $\tau\left(\varepsilon\right)$ is considered. To account such a difference, we further introduce a parameter $q = \tau_2/\tau_1$ and consider it hereinafter as a fitting parameter. In this case we obtain the following transcendental equations to calculate the effective electrical conductivity σ_e and the effective coefficient β_e, respectively:

$$\int\limits_{-\infty}^{\infty} dt \exp\left(-\frac{1}{2}t^2\right) \frac{\int_t^{\infty} dt_1 \frac{(2/3) x^{5/2} \left(t_1 - t\right)^{3/2}}{1+\exp\left[x\left(t_1 - x_F\right)\right]} \left[1 - \frac{1}{1+\exp\left[x\left(t_1 - x_F\right)\right]}\right] - X_e}{\int_t^{\infty} dt_1 \frac{(2/3) x^{5/2} \left(t_1 - t\right)^{3/2}}{1+\exp\left[x\left(t_1 - x_F\right)\right]} \left[1 - \frac{1}{1+\exp\left[x\left(t_1 - x_F\right)\right]}\right] + 2X_e} = 0 \quad (17)$$

and

$$\int\limits_{-\infty}^{\infty} dt \exp\left(-\frac{1}{2}t^2\right) \frac{\int_t^{\infty} dt_1 \frac{(2/3) x^{7/2} \left(t_1 - t\right)^{3/2} \left(t_1 - x_F\right)}{1+\exp\left[x\left(t_1 - x_F\right)\right]} \left[1 - \frac{1}{1+\exp\left[x\left(t_1 - x_F\right)\right]}\right] - Y_e}{\int_t^{\infty} dt_1 \frac{(2/3) x^{7/2} \left(t_1 - t\right)^{3/2} \left(t_1 - x_F\right)}{1+\exp\left[x\left(t_1 - x_F\right)\right]} \left[1 - \frac{1}{1+\exp\left[x\left(t_1 - x_F\right)\right]}\right] + 2Y_e} = 0 . \quad (18)$$

Here $X_e = \sigma_e/\sigma_0$, $\sigma_0 = e\mu_0 D_0 \left(k_B T\right)^{3/2}$, $\mu_0 = e\tau_1/m*$, $x = \delta/k_B T$, $x_F = \varepsilon_F/\delta$, $Y_e = \beta_e/\beta_0$, $\beta_0 = \left(k_B/e\right) q\sigma_0$, $q = \tau_2/\tau_1$.

The effective Seebeck coefficient α_e can then be obtained as

$$\alpha_e = -\frac{\beta_e}{\sigma_e} = -\alpha_0 \frac{Y_e}{X_e} , \quad (19)$$

where $\alpha_0 = (k_B/e)q$. The effective mobility $\mu_e = \sigma_e/en$ in this system can be defined by the following expression:

$$\mu_e = \mu_0 D_0 (k_B T)^{3/2} X_e/n . \quad (20)$$

It worth noting that in the limiting case of the absence of random band-edge variations ($\delta \to 0$), i.e., for the system devoid of the disorder, the present model yields the result approaching the well-known relation for the Seebeck coefficient α_e for a crystalline material [38,39]:

$$\alpha_e = -\frac{k_B}{e}\left\{-\frac{\varepsilon_F}{k_B T} + q\frac{1}{k_B T}\frac{\int_0^\infty \varepsilon^{5/2} f(\varepsilon)[1-f(\varepsilon)]d\varepsilon}{\int_0^\infty \varepsilon^{3/2} f(\varepsilon)[1-f(\varepsilon)]d\varepsilon}\right\}, \quad (21)$$

where ε_F is determined from

$$n = D_0 \int_0^\infty d\varepsilon \frac{\sqrt{\varepsilon}}{1+\exp\left(\frac{\varepsilon-\varepsilon_F}{k_B T}\right)} . \quad (22)$$

Such a coincidence with the classical result for disorder-free crystalline materials [38,39] provides an additional validation of the present EMA model.

III. RESULTS AND DISCUSSION

A. Results of theoretical calculations

Let us first consider general behaviors of Seebeck coefficient predicted within the present EMA model. Here we restrict our consideration to the case of a three-dimensional transport system by using $d = 3$ in Eq. (5) and (13). Fig. 1(a) shows the carrier-concentration dependence of Seebeck coefficient α_e calculated within the present model using Eqs.(17-19) for different energy disorder parameter δ at $T = 300K$. The carrier concentration dependence α_e calculated by Eq.(21) for a disorder-free (crystalline) system is depicted by curve 1 in Fig.(1a). Since intrinsically the EMA approach has no constraints on very weak energy disorder, we have also calculated the $\alpha_e(n)$ dependence in the $\delta \to 0$ limit using Eqs. (17-19) (c.f. curves 2 to 5 in Fig. 1a). It turned out the result is remarkably close to that obtained for a crystalline material by Eq.(21) (c.f. curve 1 in Fig. 1a). Note that since EMA calculations are applicable to arbitrarily small, yet finite values of δ,

we cannot use δ=0 in Eqs. (17-19). Therefore curve 2 in Fig. 1 was calculated using δ=25 meV, that is a sufficiently small energy disorder to effectively approach the $\delta \to 0$ limit symptomatic of a crystalline material. Moreover, the present model correctly reproduces an almost linear decrease of α_e versus logarithm of carrier concentration n, although some deviation from the linearity can be seen for the case of a large disorder, δ, (curve 5 in Fig.1a).

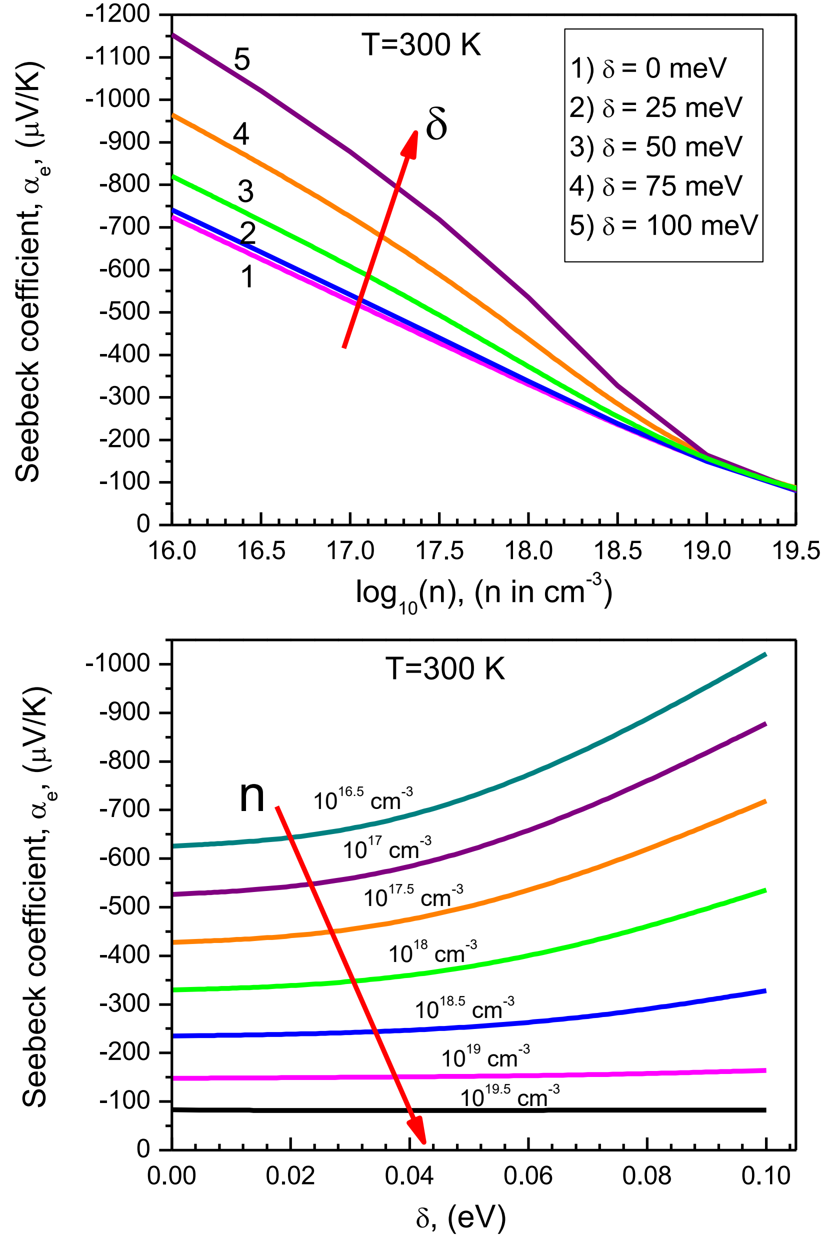

Fig. 1. (a) Carrier concentration dependences of Seebeck coefficient α_e calculated using Eqs.(17-19) for different disorder parameter δ at $T = 300\,K$ and $q = 1$ (curves 2-5). Curve 1 is calculated by Eq.(21) at $\delta = 0$ for an ordered (disorder-free) system. (b) Seebeck coefficient α_e vs. δ calculated parametric in carrier concentrations n.

Such a decrease with charge-carrier density $\alpha_e \propto -\log(n)$ is a usual behavior of Seebeck coefficient and agrees well with many experimental results [43, 44]. It has been typically interpreted by different models in terms of exponential trap DOS filling upon increasing gate voltage. We demonstrate here that this is a rather general behavior which can be reproduced in our model without invoking tail states distribution below the band edge. This seems to be well understandable because in our model the Fermi level increases within a Gaussian distribution given by Eq.(1) with increasing carrier concentration, which leads to the lowering α_e. At very high carrier concentrations (>10^{19} cm^{-3}) all curves merge (Fig. 1a) due to strong degeneracy of the semiconductor.

Further, as expected, the Seebeck coefficient increases with increasing the energy disorder parameter δ (Fig. 1b), that is typically observed experimentally and predicted by other theoretical models as well. It is normally explained by a lowering of the Fermi level as the disorder increases. However, the effect $\alpha_e(\delta)$ becomes progressively less pronounced as carrier concentration increases (Fig. 1b) and virtually vanishes at n>10^{19} cm^{-3}. This is due to strong degeneracy of the semiconductor at very large carrier concentration.

Carrier concentration dependence of the Seebeck coefficient $\alpha_e(n)$ calculated at different temperatures within the present model at δ=75 meV are presented in Fig. 2a. First, the present model does predict a rather weak temperature dependence of the Seebeck coefficient within the range of large carrier concentrations (of the order of 10^{18} cm^{-3} - a typical concentration for operating FETs), which is consistent with experimental results for a-IGZO. Second, Fig. 2a reveals an amazing effect, namely a crossover of Seebeck coefficient from a negative temperature dependence $(d\alpha_e/dT < 0)$ observed at lower carrier densities to a positive temperature dependence $(d\alpha_e/dT > 0)$ at higher concentrations (temperature change from 200 to 350 K is indicated by red arrows in Fig. 2a). This crossover occurs at concentration n_{cr} ~2×10^{18} cm^{-3} for system with δ=75 meV, implying thus an existence of a certain carrier density at which Seebeck coefficient is virtually temperature independent (the turnover point n_{cr} is shown in Fig.2a).

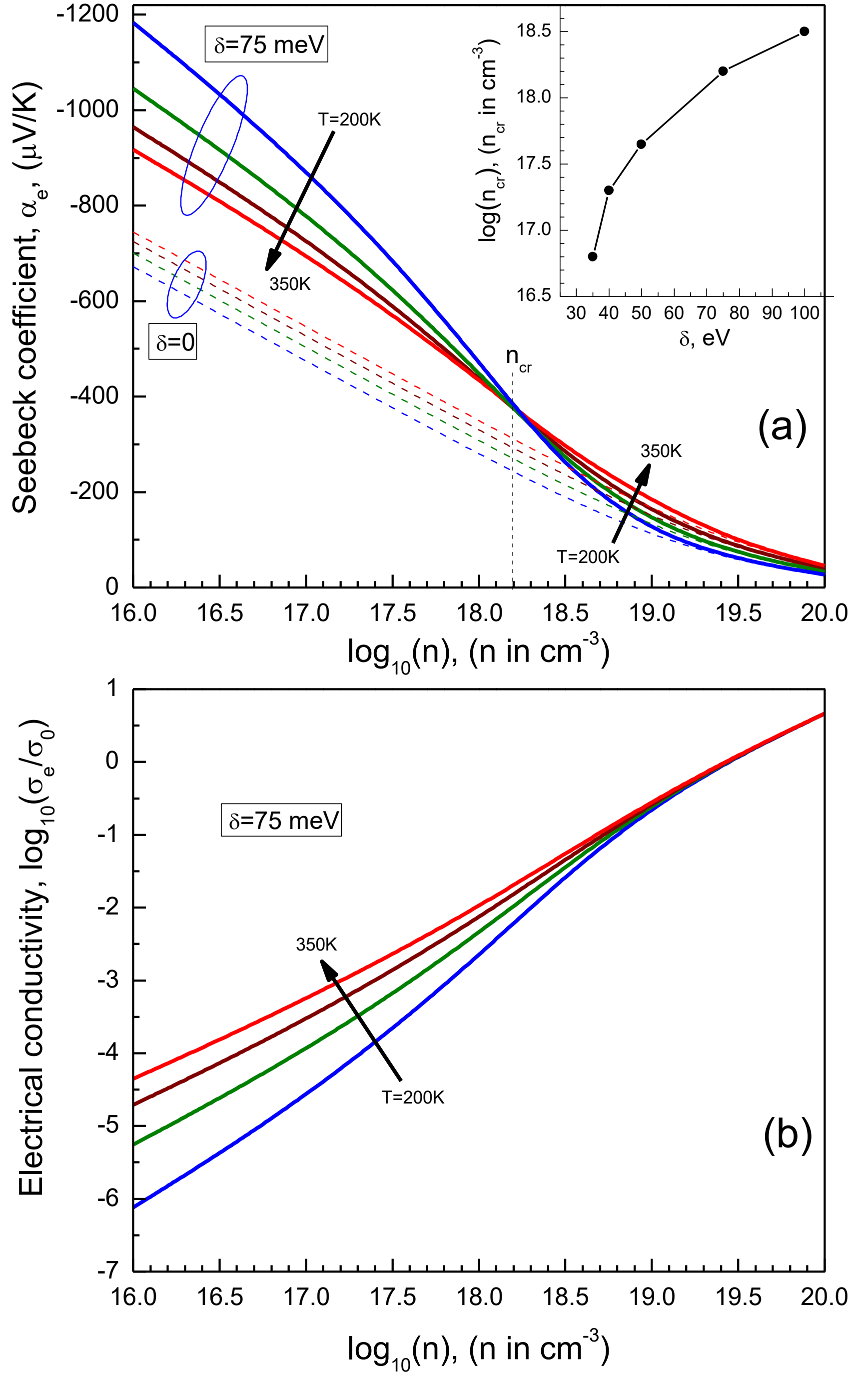

Fig. 2. (a) Seebeck coefficient α_e vs. carrier concentration ($\alpha_e \propto \log(n)$) calculated at different temperatures for an amorphous system using Eqs.(17-19) at δ=75 meV and $q = 1$ (solid lines) and for a crystalline system (δ=0) using Eq.(21) (thin dashed lines). Temperature change from 200 to 350 K in 50 K steps is shown by arrows. The turnover of the calculated dependences at n_{cr} is marked by a vertical dashed line. Inset: the turnover point n_{cr} vs. δ. (b) Electrical conductivity vs. carrier concentration (in Log-Log representation) calculated for the same amorphous system using Eq.(17).

Although both temperature dependences of $\alpha_e(T)$ have been demonstrated in literature for different materials [45-47], the emergence of the above turnover effect in the same material upon increasing carrier density (Fig. 2a) has never been reported before and therefore still needs experimental verification. We believe this result is not an artifact of the calculation. Interestingly, that similar effect has been predicted by the thermoelectric model of Kim and Pipe [47] for organic semiconductors. The authors found a similar turnover in $\alpha(T)$ from a $\alpha_e \sim 1/T$ dependence inherent to *low carrier concentration* regime and strong localization, to approximately linear dependence $\alpha_e \sim T$ in *high carrier concentration* regime and larger delocalization. This was associated to a different $\alpha(T)$ dependences that has been observed experimentally in different organic materials. Consequently, a temperature independent $\alpha_e \sim const.$ is found in the intermediate regime [47]. It is noteworthy that, Germ et at. [48] have experimentally observed a similar changeover in the temperature dependence of Seebeck coefficient measured in the same pentacene TFT at different gate voltages. The authors of Ref. [47] considered a hopping charge transport within a Gaussian DOS, but the present calculation offers a more general explanation for a similar behavior in $\alpha(T)$. Indeed, the Seebeck coefficient presented in Fig. 2a was found to follow a perfect $\alpha \propto 1 / T^2$ temperature dependence for carrier densities below $n_{cr} \sim 2\times10^{18}$ cm^{-3} (not shown here) and features approximately linear increase with increasing temperature in the range of higher carrier concentrations. It should be mentioned that Monte-Carlo simulations of $\alpha(T)$ by Tessler [46] for a hopping transport organic system with carrier density n = 10^{17} cm^{-3} yielded Seebeck coefficient decreasing with temperature as $\alpha \propto 1 / T^p$, where p is between 1 and 2 (c.f., Fig. 2a in [46]).

The above turnover effect for the temperature dependence of $\alpha(T)$ (Fig.2) in our model is directly related to the presence of energy disorder in the material. We checked it for different δ parameters, and the effect becomes progressively less and less pronounced upon reducing the disorder and practically vanishes at δ as small as 25 meV, when $\alpha(n)$ dependences no longer intersect (not shown here). In this case, $\alpha_e(T)$ features just a weak positive temperature dependence, as expected for disorder-free crystals (thin dashed lines in Fig. 2a). Interestingly, the turnover point (n_{cr}) of the temperature dependence $\alpha(T)$ clearly changes with energy disorder (inset in Fig. 2a), because n_{cr} shifts towards higher carrier concentration with increasing δ . This offers a possibility to infer the energy disorder parameter from the n_{cr} Figure 2b shows Log-Log plot of normalized electric conductivity (σ_e/σ_0) versus carrier concentrations calculated by Eq.(17) at different temperatures in the same amorphous system with δ=75 meV. As expected, the calculated conductivity features a stronger dependence on carrier concentration when temperature is lower, which is due to the

carrier-concentration dependence of the charge-carrier mobility that becomes progressively stronger with lowering temperature (not shown here).

B. Comparison with experimental results

Further, to verify applicability of the present model to a-IGZO, we fit the model to representative experimental results on the FET mobility and Seebeck coefficient measured in the same TFT device by Germs et al. [14]. Figure 3 shows the charge-carrier mobility as a function of the gate voltage ($V_G - V_{TH}$), where V_{TH} is the threshold voltage. The FET mobility was obtained in the linear regime (V_D = 2V) from the transfer characteristics measured in an a-IGZO TFT (symbols) at different temperatures [14]. The mobilities calculated by the present model using both Eq. (17) for the electrical conductivity and the relation $\mu_e = \mu_0 D_0 \left(k_B T\right)^{3/2} X_e / n$ are presented by red solid lines in Fig. 3. The total carrier concentration n is assumed to depend linearly upon the applied gate voltage V_G as $n = \phi(V_G - V_{TH})$, where $\phi = 2 \times 10^{17}$ cm^{-3}/V is a coefficient relating effective carrier concentration to the gate voltage, and $D_0 = 10^{21} cm^{-3} eV^{-3/2}$ was taken following [37]. The only fitting parameters in Fig. 3 were the band-edge disorder δ=70 meV (same as in Ref.[21]), the conduction-band mobility μ_0=19.4 cm^2/Vs taken for simplicity as a constant, and the coefficient ϕ. We did not consider here temperatures below 200 K, as the EMA approach is applicable at not too large degree of the energy disorder $\delta / k_B T$. For large $\delta / k_B T$, percolation theory is commonly believed to be the most appropriate method [21]. Fig.3 demonstrates that, despite the above simplifications, the present model reproduces correctly the relative change in the charge mobility value with changing temperature from 200 to 350K and an increase of μ_e with increasing gate voltage at $(V_G - V_{TH}) > V_D$ assuming a very reasonable carrier concentration range around ~10^{18} cm^{-3}.

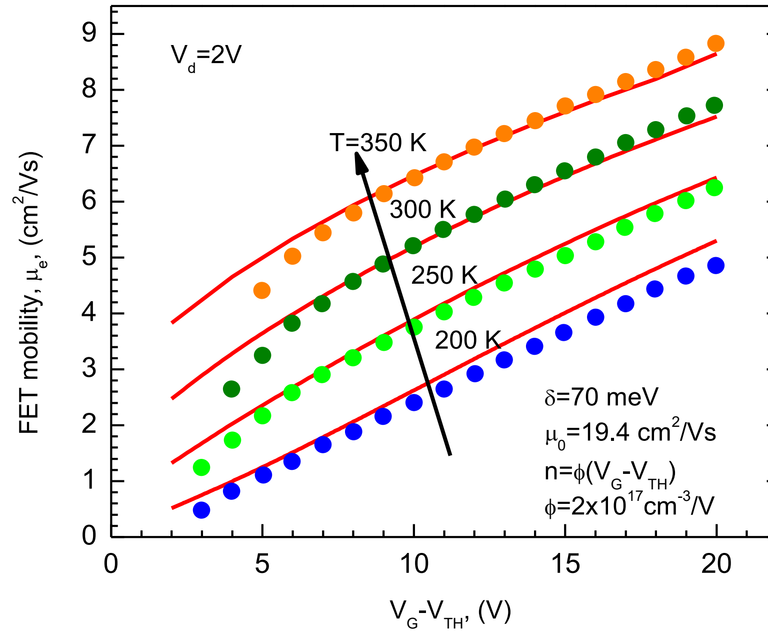

Fig. 3. Dependence of the effective FET mobility μ_e on the gate voltage ($V_G - V_{TH}$) parametric in temperatures. Symbols: experimental data from [14]. Solid lines: calculated using the present model (Eq(17)).

Next, we use the same parameters, as obtained above from the analysis of the FET mobility in Fig.3 and fit our model to the Seebeck coefficient data measured in the same a-IGZO TFT [14]. Both measurements (symbols) and calculations using Eqs.(17–19) (solid lines) of the Seebeck coefficient vs. gate voltage for different temperatures are presented in Fig.4. As can be seen, the present model provides a good quantitative description for the decrease of α_e measured in a-IGZO with increasing V_G using $q = 0.78$, while the rest of fitting parameters were the same as in Fig. 3. It also reproduces reasonably well a weak temperature dependence of the Seebeck coefficient, in particular at large V_G where a weak positive $\alpha_e(T)$ dependence is observed. Unfortunately, because of significant data scattering for the measured α_e values, especially at lower V_G, it is hard to judge whether or not the turnover from a positive temperature dependence of α_e to a negative one really occurs in a-IGZO. This issue requires a more systematic experimental study which is beyond the scope of the present study.

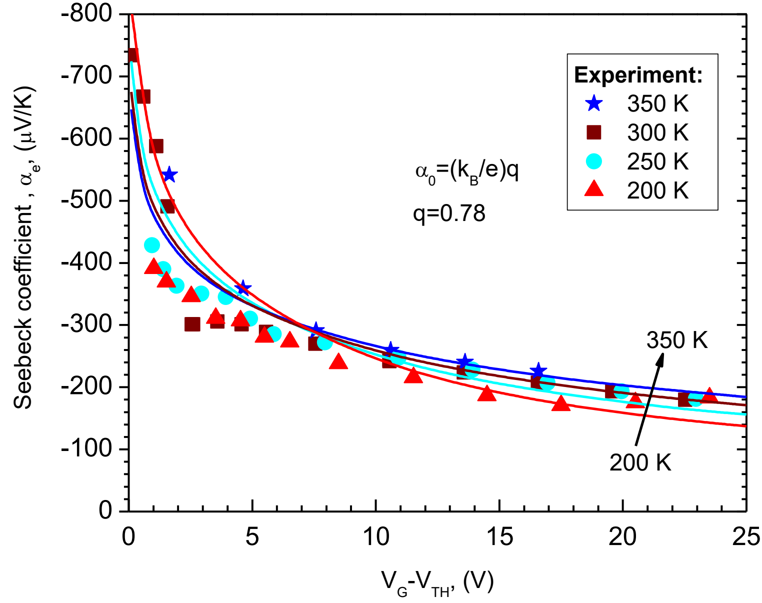

Fig. 4. Comparison between calculations and experimental field-effect-modulated Seebeck coefficient vs $(V_G - V_{TH})$ measured in a-IGZO TFT at different temperatures. Symbols: experimental data from [14]. Solid curves are calculated using Eqs. (17), (18), and (19) and parameter $q = 0.78$. All fitting parameters were the same as in Fig. 3 for the charge mobility.

C. Power Factor consideration

Having calculated Seebeck coefficient α_e and electrical conductivity σ_e (c.f. Fig. 2a and 2b), it is of obvious interest to also consider the Power Factor (PF) within the present random band-edge model. PF represents the electrical contribution to the thermoelectric generation, and it is defined as the product of the square of the Seebeck coefficient and the electrical conductivity: $PF = \alpha_e^2 \sigma_e$. Results in Fig. 2a and 2b suggest that there should be a tradeoff between the α_e and σ_e under variation of the carrier concentration, in order to maximize PF. This implies an existence of the "optimal carrier density" at which PF has a maximum value. Fig. 5a shows the calculated carrier-concentration dependence of $PF(n)$, parameterized by the energy disorder parameter δ. From these results, PF increases along with n and reaches a maximum at the carrier concentration ranging from 2×10^{19} to 7×10^{19} cm^{-3} (indicated by vertical arrows in Fig. 5a) when the energy disorder increases from δ=25 to 125 meV, respectively. Interestingly, this calculated optimal carrier density is consistent with the value of 7.7×10^{19} cm^{-3} obtained experimentally for a-IGZO films sputtered under various oxygen flow ratios [8,42]. Fig. 5b presents the power factor calculated at different temperatures, while fixed δ=75 meV. These results demonstrate that the PF

value increases significantly with increasing temperature (Fig. 5b), while the optimal carrier concentration appears to be almost independent on temperature. Note that very similar temperature behavior of PF has been observed experimentally in a-IGZO films prepared under various oxygen flow ratios to modulate free carrier concentration in the films [42].

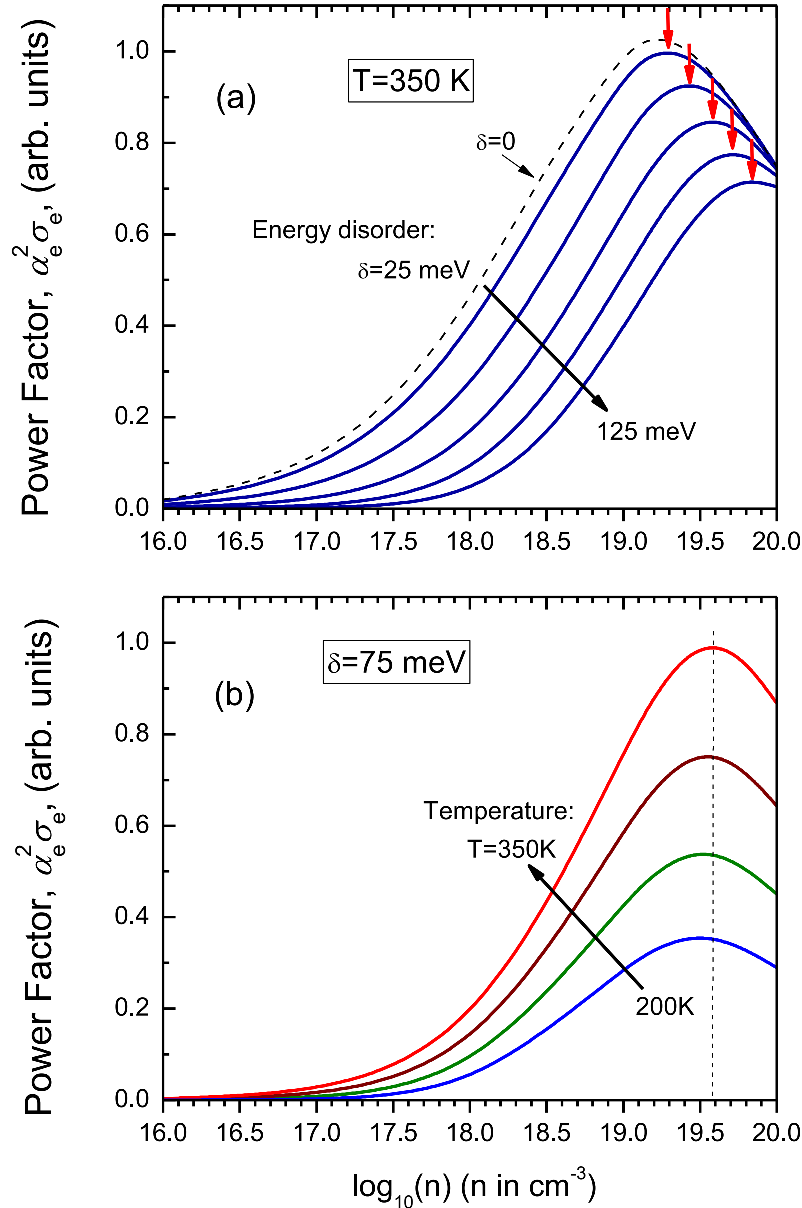

Fig. 5. The normalized power factor (solid curves) calculated as a function of carrier concentration for different energy disorder (δ) at constant T=350 K (a), and for different temperatures at constant δ=75 meV (b). δ change in 25 meV steps and temperature change from 200 to 350 K in 50 K steps, is shown by arrows in (a) and (b), respectively. Dashed curve in (a) depicts the power factor for a crystalline system (δ=0).

Further, Fig. 5a demonstrates a clear increase of the PF with decreasing δ, and the effect is relatively more pronounced at lower carrier concentrations as compared to the very high

concentration (e.g., 10^{20} cm^{-3}) where the calculated $PF(n)$ curves tend to merge. This suggests that the reduction of the energy disorder in amorphous oxide films leads to a two-fold benefit for the power factor, namely, (i) to increasing PF value, and (ii) reducing the optimal carrier concentration (Fig.5a). Such phenomenon is well known for disordered materials and has been already documented for alloy thermoelectric materials [49]. Moreover, similar effect of the energy disorder on $PF(n)$ dependence was observed in calculations within the thermoelectric model of Kim and Pipe (c.f. Fig. 3a in [47]) in the regime of hopping transport inherent to organic semiconductors. It is gratifying that predictions of present EMA model, which are based on random band-edge concept ignoring any localized states, agree qualitatively well with the results obtained for disordered materials by previous theoretical treatments .

Finally, we should comment that, although the reduction in the energy disorder in a-IGZO films leads to an increase in the power factor, a certain disorder might still be beneficial to maximize the efficiency of thermoelectric material (by improving its figure of merit) via a desired reduction of its lattice thermal conductivity. It is known that glassy materials exhibit lowest as compared to crystalline system thermal conductivity due to disrupting the phonon path, whereas their charge mobilities are typically significantly lower compared to their crystal counterparts. It is believed that an ideal thermoelectric material should be capable of scattering phonons (phonon-glass requirement of reaching as low lattice thermal conductivity as possible) without significant disruption of electrical conductivity (electron-crystal requirement of preserving a crystalline electronic structure to reach maximal power factor) [49]. A unique feature of a-IGZO is that its charge transport is less prone to disruption by material amorphization. This makes this material particularly promising for thermoelectric application as it might potentially allow realization of the concept of a 'phonon-glass electron-crystal' system [49].

D. Thermoelectric figure of merit

The thermoelectric performance of a material is generally benchmarked by the dimensionless thermoelectric figure of merit (zT) which corresponds to the generated power per the dissipated heat. The effective figure of merit $(zT)_e$ can be expressed as

$$(zT)_e = \frac{\sigma_e \alpha_e^2 T}{k_L + k_e}, \tag{23}$$

where k_L and k_e is the lattice- and electronic thermal conductivity, respectively. The electronic thermal conductivity k_e being determined under open circuit conditions can be represented as

$k_e = k_{0e} - \sigma_e \alpha_e^2 T$, where k_{e0} is the same quantity determined under short circuit conditions [50]. The effective value k_{0e} can be calculated within the framework of EMA using the following self-consistency equation:

$$\left\langle \frac{k_0(\varepsilon_m) - k_{0e}}{k_0(\varepsilon_m) + (d-1)k_{0e}} \right\rangle = 0. \tag{24}$$

In this case

$$k_0(\varepsilon_m) = \frac{2k_B}{3em^*} \frac{D_0}{(k_B T)^2} \langle \tau(\varepsilon_m) \rangle_3 \int_{\varepsilon_m}^{\infty} (\varepsilon - \varepsilon_m)^{3/2} (\varepsilon - \varepsilon_F)^2 f(\varepsilon)[1 - f(\varepsilon)] d\varepsilon, \tag{25}$$

where

$$\langle \tau(\varepsilon_m) \rangle_3 = \frac{\int_{\varepsilon_m}^{\infty} (\varepsilon - \varepsilon_m)^{3/2} \tau(\varepsilon)(\varepsilon - \varepsilon_F)^2 f(\varepsilon)[1 - f(\varepsilon)] d\varepsilon}{\int_{\varepsilon_m}^{\infty} (\varepsilon - \varepsilon_m)^{3/2} (\varepsilon - \varepsilon_F)^2 f(\varepsilon)[1 - f(\varepsilon)] d\varepsilon}. \tag{26}$$

As a result, we obtain the following transcendental equation to calculate the effective value k_{0e}

$$\int_{-\infty}^{\infty} dt \exp\left(-\frac{1}{2}t^2\right) \frac{\int_t^{\infty} dt_1 \frac{(2/3)x^{9/2}(t_1 - t)^{3/2}(t_1 - x_F)^2}{1 + \exp[x(t_1 - x_F)]} \left[1 - \frac{1}{1 + \exp[x(t_1 - x_F)]}\right] - Z_e}{\int_t^{\infty} dt_1 \frac{(2/3)x^{9/2}(t_1 - t)^{3/2}(t_1 - x_F)^2}{1 + \exp[x(t_1 - x_F)]} \left[1 - \frac{1}{1 + \exp[x(t_1 - x_F)]}\right] + 2Z_e} = 0. \tag{27}$$

Here $Z_e = k_{0e}/k_0$, where $k_0 = \sigma_0 (k_B/e)^2 q_1 T$ and $q_1 = \tau_3/\tau_1$. Similar to the calculations presented above in Section II, we assume a constant electron scattering time $\langle \tau(\varepsilon_m) \rangle_3 = \tau_3$ by setting $\varepsilon_m = 0$ in Eq. (26) and consider q_1 also as a fitting parameter. One can rewrite Eq.(23) using Eqs.(17, 19, and 27) in the following form

$$(zE)_e = \frac{Y_e^2/X_e}{1/B + Z_e(q_1/q^2) - Y_e^2/X_e}, \tag{28}$$

where $B = \frac{\left[\sigma_0 \left(\frac{k_B}{e}\right)^2 q^2 T\right]}{k_L}$ is the dimensionless thermoelectric material quality factor (also called as B-factor) [50-52] which is inversely proportional to the lattice thermal conductivity k_L. Since theoretical consideration of the lattice thermal conductivity k_L in an amorphous semiconductor is beyond the scope of the present study, we calculate $(zT)_e$ parametric in B-factor.

Fig. 6 presents the carrier-concentration dependence of the effective thermoelectric figure of merit $(zT)_e$ calculated by Eq.(28) at T=300 K for different fixed values of B at a constant energy

disorder δ. As expected, $(zT)_e$ significantly enhances with increasing B-factor (i.e., with a decrease of the lattice thermal conductivity k_L). It is evident from Fig. 6 that the $(zT)_e(n)$ dependences feature a maximum at a certain optimal carrier concentration, which somewhat shifts towards lower concentrations as B factor increases. Similar behavior has been commonly observed for various thermoelectric materials [50, 52]. Finally, we should note that $(zT)_e$ is expected to depend significantly on the energy disorder δ. However, such a calculation would require assessing the impact of the disorder on the lattice thermal conductivity k_L, which is not a trivial task and is beyond the scope of the present study.

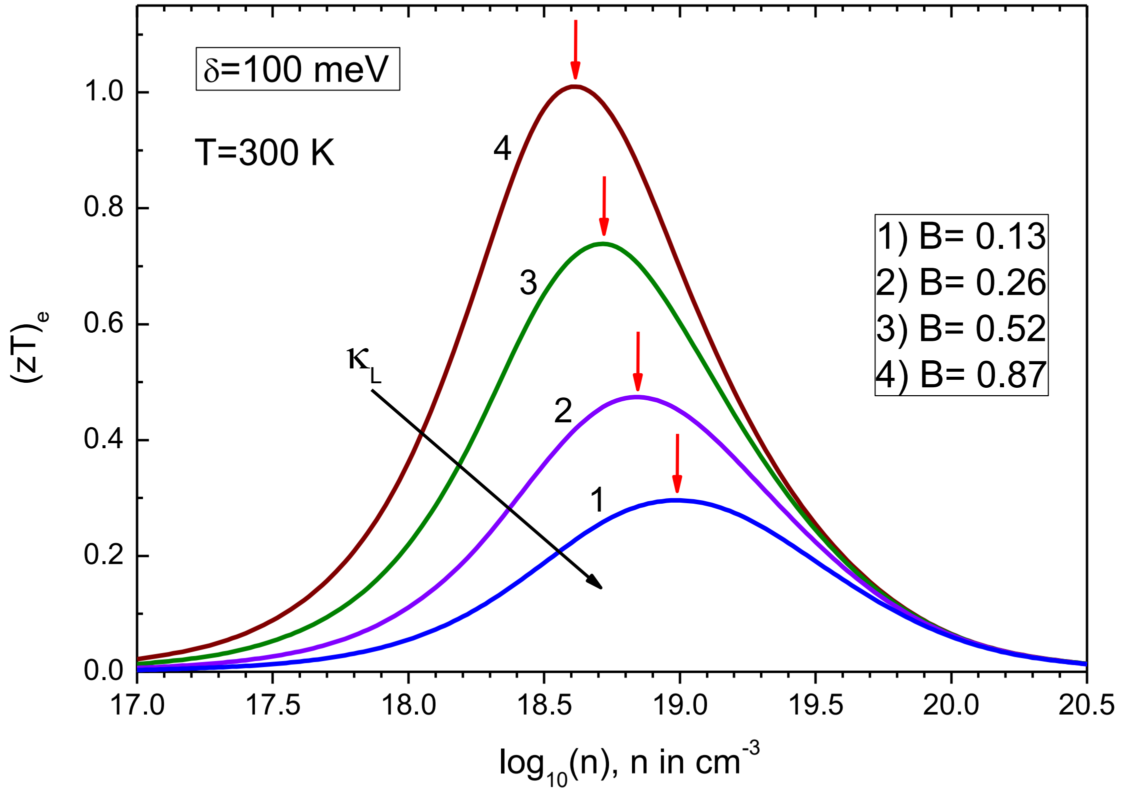

Fig. 6. The effective thermoelectric figure of merit $(zT)_e$ calculated as a function of carrier concentrations in an amorphous system at T=300 K for different B-factors at δ=100 meV. For simplicity, we assume q= q_1=1 in these calculations.

IV. CONCLUSIONS

A relatively simple physical analytic model based on an EMA framework and the random band-edge concept has been suggested to describe simultaneously both the charge-carrier mobility and thermopower in *high-mobility disordered semiconductors* as a function of carrier concentration, energy disorder and temperature. Our model considers a delocalized charge transport in the presence of variations of the conduction band edge and neglects localized tail states in the gap. The above concept is premised on the assumption that the disorder potential causes random long-

range variations of the band edge, which can be described by a Gaussian distribution with standard deviation δ, which is the key parameter of the model and is a measure of the band-edge energy disorder. The principal predictions of this model are the following: (i) the charge mobility and Seebeck coefficient can be well described within the same theoretical formalism using the same material parameters; (ii) Seebeck coefficient α_e decreases directly with the logarithm of the carrier concentration ($\alpha_e \propto -\log(n)$); (iii) since EMA approach has no constraints on very weak energy disorder, in the $\delta \to 0$ limit our model yields the $\alpha_e(n)$ dependence approaching that for disorder-free crystals; (iv) α_e increases significantly with increasing δ carrier densities, while pronunciation of the effect depends significantly on carrier concentration and it almost vanishes at very large carrier density; (v) there is a remarkable carrier-density mediated turnover effect from a negative temperature dependence ($d\alpha_e/dT < 0$) of Seebeck coefficient to a positive one ($d\alpha_e/dT > 0$) observed at relatively low and high carrier concentrations, respectively, the turnover effect in the $\alpha_e(T)$ dependence being directly related to the energy disorder and vanishes at sufficiently small δ; (vi) a very weak temperature dependence of Seebeck coefficient is found for the range of carrier concentrations (of order of 10^{18} cm^{-3} at δ=75 meV), relevant for TFT device operation; and (vii) the present model predicts a decrease in the optimal carrier concentration for the power factor upon reducing δ and for the thermoelectric figure of merit as B-factor increases.

The present EMA model has been applied to a-IGZO and was able to describe quantitatively well the available experimental results on charge mobilities and Seebeck coefficient measured in the same a-IGZO TFT device as function of gate voltage and temperature. It provides superior description of the thermoelectric properties in a-IGZO as compared to previous theoretical models applied to this material. Indeed, the Kamiya-Nomura model based on percolation approach of Adler [23] was already demonstrated [14] to overestimate significantly the Seebeck coefficient measured in the same a-IGZO TFTs and it predicts too strong temperature dependence $\alpha_e(T)$. Likewise, a significantly stronger $\alpha_e(T)$ dependence, as compared to the considered a-IGZO experimental data, was also obtained by MTR model [26]. The hybrid model of Germs et al. [14], which combines delocalized transport in the conduction band and charge hopping through the localized states, yields a similarly good description of the thermoelectric properties of a-IGZO. Yet, it has to postulate the dominance of hopping transport over the delocalized one in this high mobility material, which is incompatible with observation of a well-developed Hall effect inherent for a-IGZO. Our model avoids such a shortcoming. It is unified in the sense that it has a good representation of the Hall and drift mobility, electric conductivity and Seebeck coefficient.

Finally, it should be noted that present EMA model can potentially be applied to describe the field-effect modulated thermoelectricity in weakly disordered high-mobility organic semiconductors with delocalized nature of charge transporting states, as evidenced by observation of a well-developed Hall effect. The random band-edge concept has been already applied to explain a negative field dependence coupled with a positive temperature dependence of the charge mobility $\mu(T)$ observed in 2,7-dioctyl[1]benzothieno[3,2-*b*][1]benzothiophene (C8-BTBT) highly-crystalline films [36]. Generally, a positive $\mu(T)$ dependence for both drift and Hall mobility is not an unusual phenomenon for organic band-transport materials with weakly disordered systems has been reported earlier in the literature [53,54].

ACKNOWLEDGMENTS

The authors acknowledge funding through the EU Marie Skłodowska-Curie ITN TADF*life* grant (GA no. 812872). This research was also supported by the European Research Council under the ERC grant agreement no. 835133 (ULTRA-LUX), VW Foundation, and by the Natl. Academy of Science of Ukraine (Project No. VC/205) and NRFU 2020.01/0144.

References

1. D. Venkateshvaran, M. Nikolka, A. Sadhanala, V. Lemaur, M. Zelazny, M. Kepa, and H. Sirringhaus, Nature, 515, 384 (2014).
2. M. Wang, C. Bi, L. Li, S. B. Long, Q. Liu, H. B. Lv, N. D. Lu, P. X. Sun, and M. Liu, Nat. Commun. 5, 4598 (2014).
3. N. Lu, L. Li, and M. Liu, Phys. Rev. B 91, 195205 (2015).
4. K. Nomura, H. Ohta, A. Takagi, T. Kamiya, M. Hirano, and H. Hosono, Nature **432**, 488 (2004).
5. K. Myny, Nat. Electron. 1, 30, (2018).
6. M. Kimura, Jpn.J. Appl. Phys., 58, 090503 (2019).
7. M. Uenuma, K. Umeda, J. Felizco, D. Senaha, and Y. Uraoka, Flexible TEG Using Amorphous InGaZnO Thin Film. J.Electron.Mater., 48, 1971 (2019).
8. Y. Fujimoto, V. Uenuma, Y. Ishikawa, and Y. Uraoka, J.Electron.Mater, 45, 1377 (2016).
9. J. C. Felizco, V. Uenuma, M.N. Fujii, and Y. Uraoka, IEEE Electron Device Letters, 42, 1236 (2021).
10. B. Cui, L. Zheng, D. Keane, M. Bedzyk, D. Buchholz, R. Chang, X. Yu, J. Smith, T. Marks, Y. Xia, A. Facchetti, J. Medvedeva, and M. Grayson, J. Phys. Chem. C, 120, 14, 7467, (2016).

11. M. Nag, A. Bhoolokam, S. Steudel, A. Chasin, K. Myny, J. Maas, G. Groeseneken, and P. Heremans, Jpn. J. Appl. Phys. 53, 111401 (2014).
12. M. Kimura, T. Kamiya, T. Nakanishi, K. Nomura, and H. Hosono, Appl. Phys. Lett. 96, 262105 (2010).
13. S. D. Brotherton, Transparent amorphous oxide semiconductor TFTs, in *Introduction to Thin Film Transistors* (Springer International Publishing, Cham, Switzerland, 2013), Chap.9.
14. W. Chr. Germs, W. H. Adriaans, A. K. Tripathi, W. S. C. Roelofs, B, Cobb, R. A. J. Janssen, G. H. Gelinck, and M. Kemerink, Phys. Rev. B **86**, 155319 (2012).
15. T. Kamiya, K. Nomura, and H. Hosono, J. Disp. Technol., **5**, 462 (2009).
16. H. Hosono, J. Non-Cryst. Solids **352**, 851 (2006).
17. A. Takagi, K. Nomura, H. Ohta, H. Yanagi, T. Kamiya, M.Hirano, and H. Hosono, Thin Solid Films **486**, 38 (2005).
18. S. Lee, S. Park, S. Kim, Y. Jeon, K. Jeon, J.-H. Park, J. Park, I. Song, C. J. Kim, Y. Park, D. M. Kim, and D. H. Kim, IEEE Electron Device Lett. 31, 231 (2010).
19. J.-H. Park, K. Jeon, S. Lee, S. Kim, S. Kim, I. Song, J. Park, Y. Park, C. J. Kim, D. M. Kim, and D. H. Kim, J. Electrochem.Soc. **157**, H272 (2010).
20. I. I. Fishchuk, A. Kadashchuk, A. de Jamblinne de Meux, G. Pourtois, M. M. Gavrilyuk, A. Köhler, H. Bässler, P. Heremans, and J. Genoe, Phys. Rev., B **93**, 195204 (2016).
21. A. V. Nenashev, J. O, Oelerich, S. M. Greiner, A. V. Dvurechenskii, F. Gebhard, and S. D. Baranovskii, Phys. Rev. B **100**, 125202 (2019).
22. S. D. Baranovskii, A. V. Nenashev, J. O, Oelerich, S. M. Greiner, A. V. Dvurechenskii, and F. Gebhard, EPL, **127**, 57004 (2019).
23. D. Adler, L. P. Flora, and S. D. Sentuna, Solid State Commun. 12, 9 (1973).
24. S. Lee, K. Ghaffarzadeh, A. Nathan, J. Robertson, S. Jeon, C. Kim, I.-H. Song, and U.-I. Chung, Appl. Phys. Lett. 98, 203508 (2011).
25. S. Tomai, M. Nishimura, M. Itose, M. Matuura, M. Kasami, S. Matsuzaki, H. Kawashima, F. Utsuno, and K. Yano, Jpn. J. Appl. Phys. 51, 03CB01 (2012).
26. N. Lu, L. Li, P. Sun, W. Banerjee, and M. Liu, J. Appl. Phys. 116, 104502 (2014).
27. E. O. Kane, Phys. Rev. **131**, 79 (1963).
28. B. I. Shklovskii and A. L. Efros, *Electronic Processes of Doped Semiconductors* (Springer-Verlag, Berlin, 1984).
29. M. Nardone,M. Simon, I. V. Karpov, and V. G. Karpov, J.Appl.Phys. **112**, 071101 (2012).
30. J. A. Howard and R. A. Street, Phys. Rev. B **44**, 7935 (1991).

31. H. Overhof and P. Thomas, *Electronic Transport in Hydrogenated Amorphous Semiconductors* (Springer, Heidelberg, 1989).
32. U. Rau and J. H. Werner, Radiative efficiency limits of solar cells with lateral band-gap fluctuations, Appl. Phys. Lett. 84, 3735 (2004).
33. U. Rau, B. Blank, T. C. M. Müller, T. Kirchartz, Phys. Rev. Appl., 7, 044016 (2017).
34. M. A. Green, and A. W. Ho-Baillie, ACS Energy Letters, 4, 1639 (2019).
35. A. Kadashchuk, F. Tong, R. Janneck, I.I. Fishchuk, A. Mityashin, E. Pavlica, A. Köhler, P. Heremans, C. Rolin, G. Bratina, and J. Genoe, Phys. Rev. B, 96, 125202 (2017).
36. A. Köhler and Heinz Bässler. *Electronic processes in organic semiconductors: An introduction*. John Wiley & Sons, (2015).
37. T. Kamiya, K. Nomura, and H. Hosono, Appl. Phys. Lett. **96**, 122103 (2010).
38. V. L. Bonch-Bruevich, and S. G. Kalashnikov, *Physics of Semiconductors* (VEB Deutscher Verlag der Wissen-Schaften, Berlin, 1982)
39. J. M. Ziman, *Principles of the Theory of Solids* (Cambridge University Press, London, 1964).
40. S. Kirkpatrick, Rev. Mod. Phys. **45**, 574 (1973).
41. I. I. Fishchuk, A. Kadashchuk, S. T. Hoffmann, S. Athanasopoulos, J. Genoe, H. Bässler, and A. Köhler, Phys. Rev. B **88**, 125202 (2013).
42. Y. Fujimoto, M. Uenuma, Y. Ishikawa, and Y. Uraoka, AIP Advances **5**, 097209 (2015).
43. K. P. Pernstich, B. Rossner and B. Batlogg, Nat. Mater., 2008, 7, 321–326.
44. A. Shakouri, Annu. Rev. Mater. Res. 41, 399 (2011).
45. N. Lu, L. Li, and M. Liu, Phys.Chem.Chem.Phys. 18, 19503 (2016).
46. D. Mendels, & N. Tessler, J. Phys. Chem. Lett., 5, 3247 (2014).
47. G. Kim and K. P. Pipe, Phys. Rev. B, 86, 085208 (2012).
48. W. Chr. Germs, K. Guo, R. A. J. Janssen, and M. Kemerink, Phys. Rev. Lett., 109, 016601 (2012).
49. G. Snyder and E. Toberer, Nature Mater., 7, 105 (2008).
50. E. Witkoske, X. Wang, J. Maassen, M. Lundstrom, Mater. Today Phys, 8, 43 (2019).
51. G.D. Mahan, J. Appl. Phys. 65, 1578 (1989).
52. S.D. Kang, G.J. Snyder, Transport Property Analysis Method for Thermoelectric Materials: Material Quality Factor and the Effective Mass Model, 2017, pp. 1-5. http://arxiv.org/abs/1710.06896.
53. J.-F. Chang, T. Sakanoue, Y. Olivier, T. Uemura, M.-B. Dufourg-Madec, S. G. Yeates, J. Cornil, J. Takeya, A. Troisi, and H. Sirringhaus, Phys. Rev. Lett. **107**, 066601 (2011).

54. S. Haas, A. F. Stassen, G. Schuck, K. P. Pernstich, D. J. Gundlach, B. Batlogg, U. Berens, and H.-J. Kirner, Phys. Rev. B **76**, 115203 (2007).